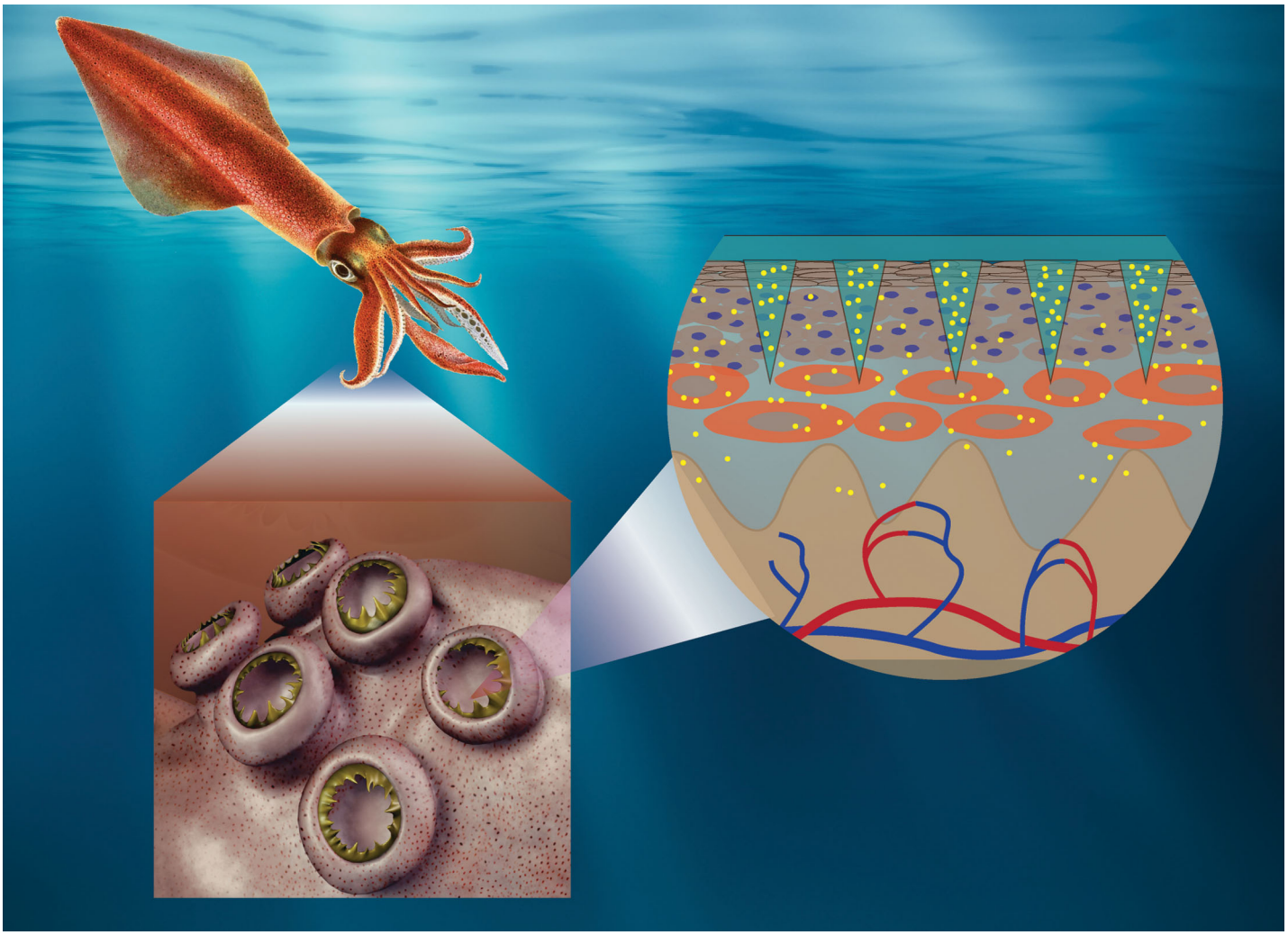

Showcasing research from the Biological and Biomimetic Materials Laboratory (Prof. Ali Miserez's research team) in the School of Materials Science and Engineering, Nanyang Technological University, Singapore.

Squid suckerin microneedle arrays for tunable drug release

Sucker ring teeth from squids' tentacles are supramolecular protein biopolymers that can be solubilized and re-shaped into micro-needle arrays by soft lithography. Drugs can be loaded within the micro-needles and their release profile through the skin is pH-dependent.

As featured in:

See Lifeng Kang, Ali Miserez *et al.*, *J. Mater. Chem. B*, 2017, **5**, 8467.

ROYAL SOCIETY OF CHEMISTRY

rsc.li/materials-b

Registered charity number: 207890

Journal of Materials Chemistry B

PAPER

View Article Online
View Journal | View Issue

Check for updates

Cite this: J. Mater. Chem. B, 2017, 5, 8467

Squid suckerin microneedle arrays for tunable drug release†

Dawei Ding,[a] Jing Pan,[b] Seng Han Lim,[b] Shahrouz Amini,[a] Lifeng Kang ‡*[b] and Ali Miserez *[ac]

Microneedles are increasingly used in transdermal delivery of therapeutic agents due to the elimination of first-pass metabolism, simplicity of operation, and lack of pain, which collectively lead to improved patient compliance. However, microneedles are still met by challenges with regard to the choice of biocompatible materials and the control of drug release profiles. Herein, we tackle these limitations by producing microneedles from a biocompatible robust biopolymer, namely squid sucker ring teeth (SRT) proteins (suckerins), using a soft lithography method. Taking advantage of the modular sequence design of suckerins leading to their self-assembly into β-sheet enriched structures, suckerin microneedles display an accurate replication of their templates with robust mechanical properties, endowing them with a high skin penetration capability. Critically, the β-sheet content in the microneedles can be modulated by varying the solvent conditions, which allows tuning of the mechanical response, and in turn the drug release rates by more than one order of magnitude. *In vitro* skin permeation studies of suckerin microneedles using human cadaver skin samples suggest a fast onset and enhanced skin permeation of drugs compared to flat patches. The skin permeation can also be tailored 10-fold by applying hydrogen bond disruptor solutions. As a proof-of-concept, the anti-bacterial drug kanamycin is encapsulated within the microneedles, leading to efficient anti-bacterial activity and offering an additional benefit to further minimize the risk of infections caused by microneedle-based drug delivery systems. Lastly, suckerin microneedles are found to be biocompatible in cell culture studies, opening the door to further clinical applications.

Received 5th June 2017,
Accepted 11th September 2017

DOI: 10.1039/c7tb01507k

rsc.li/materials-b

Published on 12 September 2017. Downloaded on 15/11/2017 07:40:57.

Introduction

Transdermal drug delivery has been established as an attractive and widely adopted approach for the delivery of therapeutic agents due to its ease of operation, the elimination of drug degradation in the gastrointestinal tract, and the avoidance of first-pass metabolism in the liver encountered with oral delivery.[1,2] It also bypasses a number of complexities arising from hypodermic injection, including pain, potential infection, the requirement of trained personnel, as well as frequent and repeated injections to patients.[3] However, owing to the stratum corneum, intact skin allows the permeation of only small and moderately hydrophobic molecules.[3,4] Consequently, microneedles are emerging as a minimally invasive alternative to increase the skin permeability for the transdermal delivery of a broad spectrum of drugs ranging from small molecules to proteins and from DNA to vaccines.[5–7] By piercing the skin with micron-scale needles, microneedle arrays offer simplicity of application and lack of pain, in turn enhancing patient compliance and eliminating bio-hazardous waste.[3,8,9]

The development of microneedles, on the other hand, has been hindered by various challenges and limitations. The first challenge is the choice of appropriate biomaterials.[4,8] An ideal material for microneedle engineering should be mechanically robust for skin penetration,[10] biocompatible, able to stabilize drugs, and should eventually degrade into non-toxic products.[3] Most microneedle arrays have been engineered with silicon, metals, ceramics and synthetic polymers (*e.g.* polycarbonate and poly-methyl-methacrylate (PMMA)).[7,11] These materials are strong enough to penetrate the skin, but are faced with safety

[a] *Center for Biomimetic Sensor Science (CBSS), School of Materials Science and Engineering, Nanyang Technological University (NTU), 50 Nanyang Avenue, Singapore 639798, Singapore. E-mail: ali.miserez@ntu.edu.sg*
[b] *Department of Pharmacy, National University of Singapore (NUS), 18 Science Drive 4, Singapore 117543, Singapore*
[c] *School of Biological Sciences, NTU, 60 Nanyang Drive, Singapore 637551, Singapore*

† Electronic supplementary information (ESI) available: Additional experimental details are provided. Images of 3D printed templates and SRT microneedles prepared accordingly are presented in Fig. S1. Sample preparation for nano-indentation testing and representative nanoindentation curves are shown in Fig. S2. Rheology data of SRT microneedles in 2M urea are displayed in Fig. S3. MALDi-ToF data of kanamycin is displayed in Fig. S4. Data of *E. coli* cultured in various conditions are presented in Fig. S5–S7. See DOI: 10.1039/c7tb01507k

‡ Current address: Faculty of Pharmacy, University of Sydney, Pharmacy and Bank Building A15, NSW 2006, Australia. E-mail: lifeng.kang@sydney.edu.au

Published on 12 September 2017. Downloaded on 15/11/2017 07:40:57.

concerns when they break off in the skin.[3] Therefore, biocompatible polymers such as poly-vinyl-pyrrolidone (PVP),[9] polyethylene glycol (PEG),[12] hyaluronic acid (HA)[13] and proteins (*e.g.* silk fibroins[8]) are receiving increasing attention for microneedle engineering. These biopolymers, on the other hand, are limited by the processing conditions and to some extent by their mechanical performance. For example, UV light and initiators employed in the fabrication of photo-curable microneedles might have an impact on the encapsulated drugs.[8] Another challenge with most microneedle-based drug delivery systems is the lack of controllability of the drug release kinetics.[8] For example, drug-coated microneedles or dissolving polymeric microneedles provide poor control over drug release other than a relatively short-term burst release.[8,9] Drug release from silk fibroin microneedles could be tailored by adjusting the crystallinity of as-prepared materials, but the process required complex water-annealing during post-processing.[8] In another example, hydrogel-forming microneedles were capable of accelerating drug permeation across skin through the combination of microneedles with iontophoresis,[14] but this process required the application of an extra electrical current for its operation. Thus, the development of mechanically robust biocompatible microneedles combining simple and mild fabrication processes with sustained release – especially stimuli-responsive release of drugs – is highly desired.

Jumbo squid (*Dosidicus gigas*) sucker ring teeth (SRT) are a recently discovered biomaterial exhibiting high mechanical properties on par with strong synthetic polymers.[15,16] Devoid of minerals, chitin and inter-protein covalent crosslinks, SRT are entirely made of structural proteins called "suckerins" that self-assemble into a robust supramolecular network containing a high amount of β-sheets as load-bearing nano-scale building blocks.[17,18] At the primary sequence level, suckerins display a block copolymer architecture composed of two repetitive domains: alanine (Ala)-rich peptide domains form nanoscale β-sheets, which are intervened by longer, mostly amorphous domains dominated by glycine (Gly) and tyrosine (Tyr) residues (Fig. 1a). Furthermore, another useful feature of suckerins is related to their relatively high histidine (His) content, notably in the β-sheet forming domains where they comprise 25 mol% of the peptide modules, whereas they are less abundant in the Gly-rich domains (Fig. 1a). Critically, SRT can be readily processed into complex macroscopic shapes using either their unique thermoplastic characteristics[19,20] or their high solubility in weak acidic solvents (such as acetic acid or formic acid), which is directly related to their biochemical characteristics as well as their supramolecular assembly. The modular design and self-assembly characteristics make suckerins intriguing biomacromolecules for a wide range of applications.[17] For example, taking advantages of β-sheet formation ability and the bias towards Tyr residues in amorphous domains, recombinant suckerin-19 has been engineered into biocompatible and mechanically tunable gels and films, where variation in di-Tyr crosslinks allowed to indirectly modulate the content of β-sheet structures, and consequently the material's mechanical response.[21]

In the present study, exploiting this combination of properties, namely ease of processing, biocompatibility, and β-sheet induced supramolecular self-assembly with high mechanical strength, we developed suckerin-based microneedle arrays for sustained and tunable drug release. Because of the abundance of His residues, suckerin chains are protonated at lower pH, which we reasoned would lead to an increase in chain mobility and to a decrease in β-sheet content.[22] In turn, the mechanical strength would be decreased in a controlled fashion, which would lead to a concomitant enhanced rate of drug release (Fig. 1b), as recently shown in mechanically tuned biopolymeric hydrogels.[23] Similarly, we reasoned that urea could also decrease the β-sheet content in suckerin microneedles, thus allowing for further modulation of drug release profile. Therefore, we anticipate that suckerin microneedles are promising candidates to tackle key limitations associated with microneedle-based transdermal drug delivery.

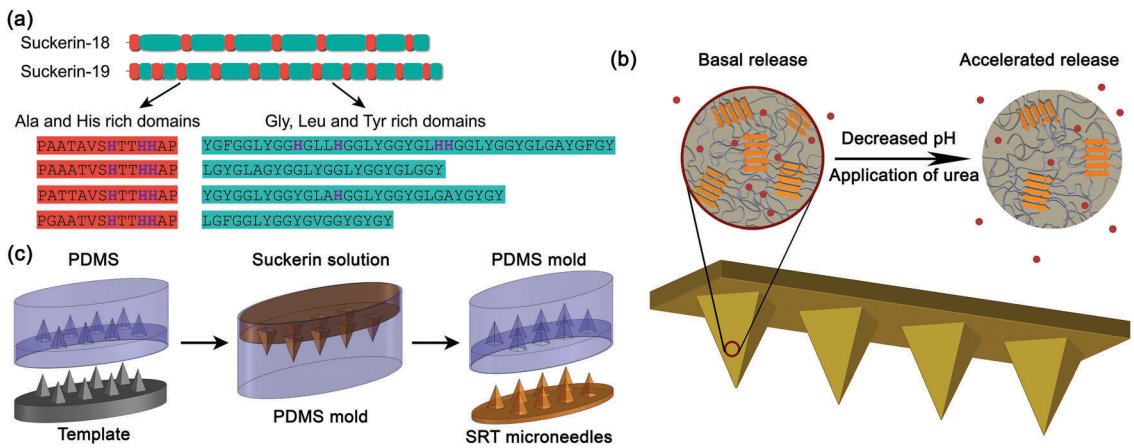

Fig. 1 (a) Modular primary structure of suckerins. Representative *D. gigas* suckerins (suckerin-18 and suckerin-19) and sub-domain peptide modules are shown. His residues are highlighted in blue for both β-sheet forming domains and amorphous domains. (b) Schematic representation of suckerin microneedles and tunability of drug release profiles from suckerin microneedles. (c) Suckerin microneedle array fabrication process. The template (3M™ Microchannel Skin System) was used to cast a PDMS negative mold. A mixture of suckerin and drug in solution was wetted over the PDMS mold and allowed to dry, eventually forming microneedles loaded with drugs.

 This journal is © The Royal Society of Chemistry 2017

Published on 12 September 2017. Downloaded on 15/11/2017 07:40:57.

Results and discussion

Fabrication and characterization of suckerin microneedle arrays

We started by preparing suckerin microneedle arrays by a facile method using soft lithography (Fig. 1c). To this end, we first chose a commercially available microneedle array, namely the 3M™ Microchannel Skin System, as the template (Fig. 2a, left), due to the well-established shape and aspect ratio of these needles for efficient skin penetration.[24] The 3M microneedle template was used to create a negative and complementary mold made of polydimethylsiloxane (PDMS) (Fig. 1c). PDMS was selected as the mold material since it is elastic, chemically stable/inert, and able to exactly reproduce the template microstructures especially at high aspect ratios. Further, its porous network allows the removal of water and volatile solvents during the molding process.[25] These characteristics endow PDMS molds with easy detachment from templates and molded products, which has led to widespread usage for molding with a broad range of polymers and solvents.[3] The PDMS molds were then utilized to fabricate the replica microneedles made of suckerins by a simple solvent evaporation method at ambient temperature. Suckerin proteins may also be shaped using thermo-forming,[19,20] but thermal processing was not utilized in this study since elevated temperatures may lead to degradation of the encapsulated drugs. 2% acetic acid was used as the protein solvent, which has been shown to be compatible with the delivery of a wide range of biomolecules including proteins.[26] Therefore, the generally mild nature of this preparation process enables the encapsulation and subsequent release of both small molecules and biomacromolecules from suckerin microneedles. It is also noteworthy that this PDMS-based fabrication process is amenable to scaling up, since it is possible to replicate one template into a dozen of PDMS molds, and then each mold could be re-used multiple times to produce tens of suckerin microneedle arrays.

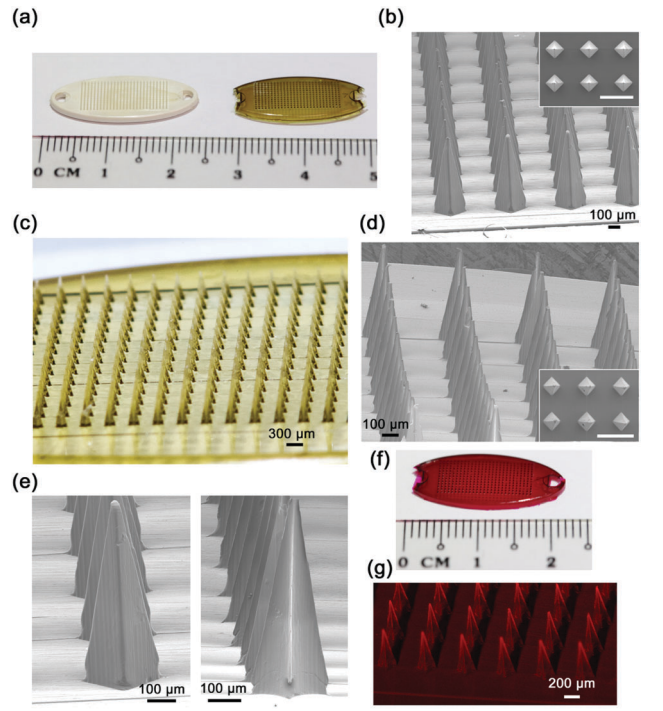

Fig. 2 (a) Macrophotos of the 3M template (left) and the suckerin microneedle arrays (right). (b) SEM micrograph of the template microneedles used to fabricate the PDMS mold. The inset shows the top view of the microneedles. The scale bar in the inset represents 500 μm. (c) Stereo micrograph of a suckerin microneedle array. (d) SEM micrograph of suckerin microneedles. The inset shows the top view of the microneedles. The scale bar in the inset represents 500 μm. (e) Zoom-in SEM micrograph of the template (left) and suckerin (right) microneedles. (f) Macrophoto of rhodamine B-loaded suckerin microneedle arrays. (g) Fluorescent image of rhodamine B-loaded suckerin microneedles.

The resulting suckerin microneedle arrays faithfully replicated the 3M template (Fig. 2a). A closer look at the suckerin microneedle arrays by optical and Scanning Electron Microscopy (SEM) imaging revealed a pyramid-like geometry, with single micro-needles featuring a height of *ca.* 650 μm and a base width of *ca.* 180 μm. The center-to-center inter-needle spacing was 500 μm, which represented an accurate replicate of the 3M templates (Fig. 2b–d and insets). The radius at the tapered end of the microneedles was around 10 μm (Fig. 2e), providing an ideal tip sharpness for skin penetration[27] as discussed below. To test the drug encapsulation ability of suckerin microneedles, the model drug rhodamine B was mixed with the suckerin protein solution. Critically, this incorporation did not affect the molding and integrity of the suckerin microneedles (Fig. 2f). We also loaded the anti-bacterial compound kanamycin in the suckerin microneedles and achieved a high payload efficiency as high as 6.25 wt%, which is higher than the loading obtained with microneedles made of silk fibroins[8] or synthetic polymers such as PVP[3] and HA.[13] Fluorescent microscopic images displayed a needle geometry which resembled that of suckerin microneedles without drugs (Fig. 2g). In addition, in order to verify the versatility of the molding process for suckerin proteins, we created a 3D-printed template (Fig. S1a, ESI†) for the replication of suckerin microneedles with customized parameters, including needle dimension, geometry, interspace and array pattern. With this technique, we were able to achieve polymeric templates and suckerin microneedle arrays that replicated the conical needle geometry of the mold, namely a center-to-center interspace of 1000 μm, a bottom diameter of ~400 μm, a needle tip radius of 30 μm, as well as a similar needle height as that prepared from the 3M template (Fig. S2b and c, ESI†). These data demonstrate a broad tunability of the fabrication process using suckerin proteins to prepare the microneedles. Based on previous reports in the literature[3,4,8,9,13,14] using the same type of microneedle geometry but with weaker polymers, it is reasonable to envision a skin penetration ability at least as good as the current benchmark, as shown below.

Skin penetration efficiency, mechanical properties and protein secondary structures

In the next step, we established the mechanical functionality of suckerin microneedles by *in vitro* penetration studies using rat skin samples. Fig. 3a shows a high skin penetration percentage near 90%, indicating that suckerin microneedles successfully

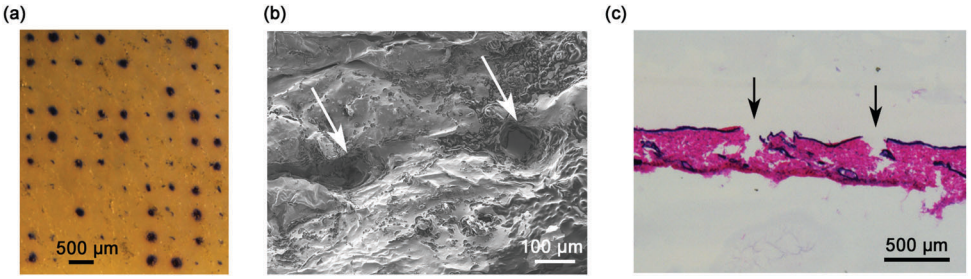

Fig. 3 (a) Skin penetration assay of suckerin microneedles. (b) SEM and (c) H&E staining micrographs of rat skin demonstrating skin penetration by suckerin microneedles. The arrows indicate skin breakage due to suckerin microneedle penetration, creating diffusion channels for the drugs.

Published on 12 September 2017. Downloaded on 15/11/2017 07:40:57.

penetrated the epidermis to access the underlying tissues. We suggest that the discrepancy in penetration depth between some of the microneedles (as illustrated by the different sizes of blue spots in Fig. 3a) is due to the slight bending of these individual microneedles replicating that of the initial template (data not shown), causing variations in actual mechanical stresses perpendicular to the skin surface. The skin penetration ability of suckerin microneedles was also supported by SEM and hematoxylin and eosin (H&E) staining, where obvious open cavities could be observed, in both the top (Fig. 3b) and side views (Fig. 3c), with the latter indicating a depth of *ca.* 250 μm. Interestingly, this depth was slightly higher than that achieved by dissolving polymer microneedles[9] in porcine skin featuring a similar thickness as human skin.[28] In other words, these data demonstrate that the suckerin microneedles provided sufficient mechanical strength to penetrate skin for drug delivery.

In order to quantitatively assess the mechanical properties of suckerin microneedles, they were probed by depth-sensing nanoindentation.[29] To mimic the stress state on the microneedles in their targeted applications, they were sectioned by ultra-microtomy perpendicular to their longitudinal axis and indented parallel to their axis (Fig. S2a, ESI†). The Young's modulus (E) of suckerin microneedles was 8.9 GPa in the dry state (Fig. 4a), which is consistent with the values of native SRT[15] and in agreement with a high skin penetration efficacy described above. This modulus is higher than that of many engineered polymers including PMMA, PEEK, or polyamides,[30] and was almost twice that of the 3M template (4.75 GPa) (Fig. 4a). Under hydrated conditions in phosphate buffer saline (PBS) at pH 7.4, E of suckerin microneedles decreased to 1.1 GPa. The decay in E was much more pronounced in pH 5 buffer (1.7 MPa), and it further decreased to values as low as 2.8 kPa in 2 M urea solution (Fig. 4a and Fig. S3, ESI†). Thus, we were able to tailor the Young's modulus of suckerin microneedles over nearly 6 orders of magnitude by simple incubation in different solutions. Since the elastic modulus of β-sheet rich protein-based polymers strongly depends on the β-sheet content, as shown for example in silk,[31,32] native SRT[18] and crosslinked recombinant suckerin based materials,[21] we hypothesized that the extensive decrease in E for suckerin microneedles could also be ascribed to differences in β-sheet content, which may be varied by incubation in solutions that target hydrogen bonds. To verify this hypothesis, we assessed the microneedle arrays by Fourier Transform Infrared (FTIR) spectroscopy in the attenuated total reflection (ATR) mode. All microneedles in different conditions exhibited the characteristic absorption peaks of β-sheets, namely 1624 cm^{-1} in the Amide I region, 1520 cm^{-1} in the Amide II region[33,34] and 1236 cm^{-1} in the Amide III region[35] (Fig. 4b). Shoulder peaks assigned to random coil structures were concurrently observed at 1648 cm^{-1} in the Amide I region and 1547 cm^{-1} in the Amide II region. Comparisons between spectra in the dry state and at pH 7.4 on the one hand, and those at pH 5 and in 2 M urea on the other hand, revealed obvious intensity increase of 1648 cm^{-1}, 1547 cm^{-1} and 1245 cm^{-1} peaks, suggesting a transition of β-sheet dominated structures towards random coil structures as pH decreases or with the addition of urea. Taken together, the data suggest a direct correlation between the elastic modulus and β-sheet content, which is consistent with the load-bearing functionality of nanoscale β-sheets in protein-based biopolymers.[32] We attribute this behavior to the molecular structure of suckerins, which consist of a di-block copolymer structure of β-sheet forming peptides intercalated by longer amorphous domains.[18,36] His residues are distributed in relatively high concentration within the β-sheet (Ala-rich) peptides, whereas their presence in amorphous (Gly and Tyr-rich) domains is much more moderate (Fig. 1a). Given that the pK_a of His is approximately 6.5, it is reasonable to suggest that decreasing the pH from 7.5 to below 5 will increase the flexibility and hydrophilicity of Ala- and His-rich domains due to the protonation of His residues, which leads to charge–charge repulsion and to partial disruption of hydrogen bonded β-sheets, and in turn to a decrease in the relative content of β-sheets. Similar disruption of hydrogen-bonded β-sheets *via* charge–charge repulsion has, for instance, recently been demonstrated in supramolecular peptides.[22] Likewise, urea is a well-known hydrogen bond disrupter capable of unfolding β-sheets in suckerin microneedles, as previously reported for native SRT.[18] Compared to the elastic properties modulation of recombinant suckerin-19 materials that was indirectly achieved by tailoring β-sheet content *via* changing the crosslinking density in the adjacent amorphous domains, the tunability obtained in this study is directly associated with partial β-sheet dissolution using external stimuli, both of which provide a versatile mechanism to tune the mechanical response of suckerin based materials.

 This journal is © The Royal Society of Chemistry 2017

Published on 12 September 2017. Downloaded on 15/11/2017 07:40:57.

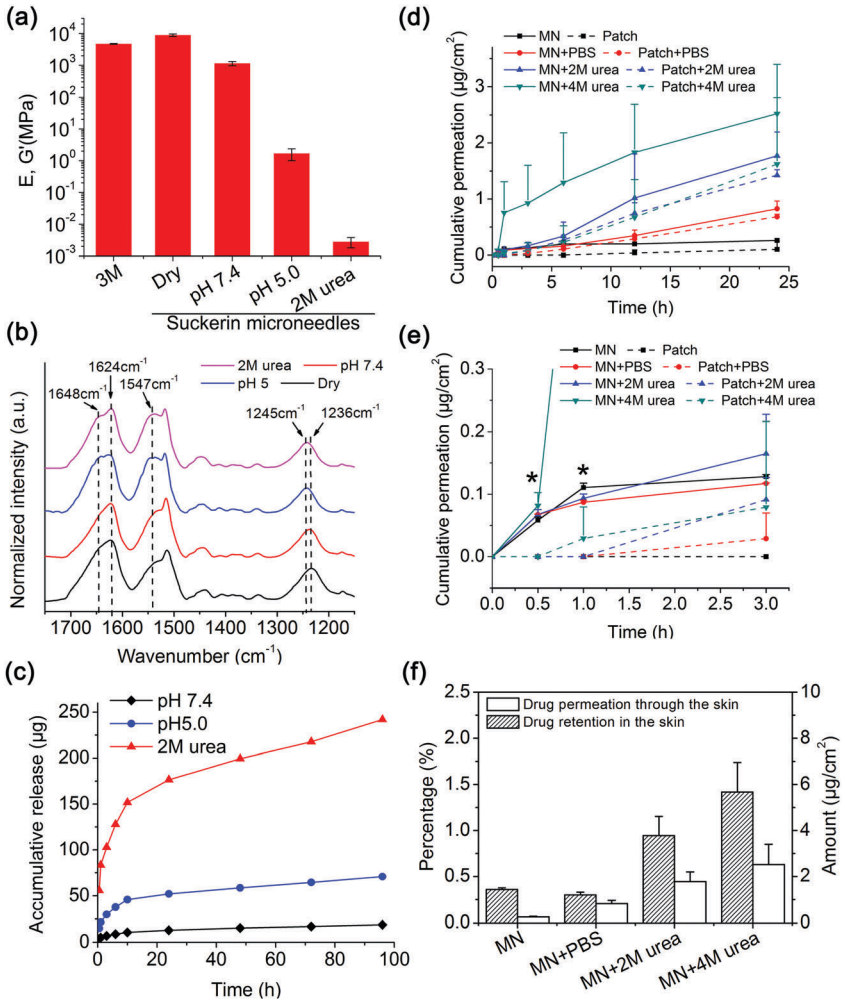

Fig. 4 (a) Mechanical properties of suckerin microneedles in different conditions obtained by depth-sensing indentation (all samples except that in 2 M urea) and by rheology (2 M urea), for which the storage modulus (G') was obtained. (b) FTIR spectra of suckerin microneedles under different conditions. (c) Release profiles of rhodamine B from suckerin microneedles under different conditions. (d) *In vitro* (human cadaver) skin permeation study of rhodamine B with suckerin microneedles compared to flat suckerin patches in different conditions. MN: suckerin microneedles. (e) Comparison of skin permeation between SRT microneedles and flat patches in the first 3 h. *$P < 0.05$ by one-way ANOVA with *post hoc* analysis. (f) Percentage and total amount of drug permeation and retention in skin for SRT microneedles with different treatments.

Drug release and skin permeation from suckerin microneedle arrays

The wide range of achievable mechanical properties provides a straightforward way to regulate the drug release profiles of suckerin microneedles, as illustrated in Fig. 4c for rhodamine B. The overall release at pH 7.4 was slow, but it accelerated more than 3-fold at pH 5, and further increased by another factor of 3 in 2 M urea, indicating a direct correlation with the mechanical response in different solutions (Fig. 4a). It should also be emphasized that while a fast release was observed in the initial 10 hours, all conditions displayed a continuous and sustained release of rhodamine B for at least 4 days. The decrease in elastic modulus in suckerin micro-needles is concomitantly associated with increased swelling (leading to an increase in chain mobility), as well as with the larger mesh size of the polymer network, both of which are strongly expected to increase the permeability for drug diffusion. A similar inverse correlation between drug release kinetics and elastic modulus was recently reported for metallo-gels whose storage modulus was tuned over several orders of magnitude by varying metal ligand valence.[23] We note that a concentration of 2 M urea (~10 wt%) matches that found in a variety of clinically used urea creams for topical applications, indicating that combining suckerin microneedles with urea creams may allow one to adjust the drug release rate more than 10-fold. To the best of our knowledge, this release kinetics modulation has not been reported in other types of biomaterial-based microneedles such as silk fibroin[8] or PEG.[12] Taken together, these data suggest a direct interplay between structure, mechanical property and drug release profile in suckerin microneedles, which can be tailored by external stimuli. Moreover, swellable microneedles have been engineered with poly-styrene cores and poly(styrene)-*block*-poly(acrylic acid) tips, which are able to adhere to and mechanically interlock soft tissues for the purpose of graft fixation.[37]

Published on 12 September 2017. Downloaded on 15/11/2017 07:40:57.

But this strategy requires harsh conditions for preparation, including using *N*,*N*-dimethylformamide (DMF) to dissolve the block co-polymer and high temperature to melt polystyrene. As suckerin microneedles also display swelling and changes in mechanical properties (*e.g.* at low pH), it is reasonable to envision their usage in similar applications, with the added advantage that suckerin proteins are easier to process under benign conditions. Avoiding harsh processing would also make it possible for suckerin microneedles to encapsulate therapeutic agents such as anti-inflammatory agents and antibiotics to facilitate wound healing besides the fixation of graft tissues. A recent study has demonstrated the ability of recombinant suckerin to encapsulate different hydrophobic drugs, with the release rate also modulated as a function of pH.[38]

Given the tunability of the drug release rate from suckerin microneedles in various conditions, an *in vitro* skin permeation test by Franz Cells[39] was conducted over a period of 24 h to investigate the practical potential of suckerin microneedles. Flat patches without microneedles were used as control. For suckerin microneedles without any additional treatment, a low amount of rhodamine B (0.26 μg cm^{-2}) permeated through human cadaver skins in dry conditions for 24 h (Fig. 4d). Application of the buffer or the urea solution accelerated skin permeation of drugs, with the permeation amount increasing 3.3 fold in PBS. Compared to PBS, urea solution further enhanced the skin permeation after 24 h by 2.1-fold with 2 M urea, and 3-fold with 4 M urea. Therefore, incubation with urea resulted in a higher amount of rhodamine that permeated through the skin. In total, a 10-fold enhancement could be achieved by applying PBS and urea solutions. These data are in agreement with the *in vitro* drug release data (Fig. 4c) and suggest that as a hydrogen bond disrupter, urea unfolds suckerin proteins[18] and disrupts the structural integrity of suckerin microneedles, thereby leading to accelerated drug diffusion. It is also important to note that 4 M urea solution (~23%, w/w) is safely within the range of commercially available urea creams in terms of urea concentration (which can be up to 40% by weight),[40] implying that skin permeation could be modulated by applying a urea cream concomitantly with suckerin microneedles. Comparing microneedles with flat patches, we obtained higher (20–50%) skin permeation of drugs from the microneedles under each condition (Fig. 4d), revealing the critical role of microneedles in creating micro-channels through the stratum corneum of the skin that enhanced the rate of drug permeation,[12] as also shown in our skin penetration studies (Fig. 3). Taking advantage of these micro-channels, rhodamine B could be detected in the receptor solution within 30 min post-application. We observed obvious differences in drug permeation in the first 3 h between microneedles and flat patches in all conditions (Fig. 4e). Almost no rhodamine B could be detected in the receptor solutions from flat patches before 3 h, and its amount was significantly lower than that from microneedles from 0.5 to 3 h. Moreover, the differences in skin permeation during this period were amplified if 4 M urea was concomitantly applied with the microneedles and patches (Fig. 4d). In other words, the lag time of rhodamine B permeation was reduced from 3 h to 30 min using suckerin microneedles. Taken together, these data suggest a faster onset of drug permeation across the skin from suckerin microneedles, which could also be beneficial for drug delivery applications. For example, it would allow for faster pain relief if a pain-killer was delivered from suckerin microneedles.[12] Finally, treatment of microneedles with PBS and urea solutions resulted in a significant increase of total drug permeated through and retained in the skin. Particularly, SRT microneedles that were treated with 4 M urea achieved a total amount of 8.19 μg cm^{-2} rhodamine B permeated through and retained in the skin within 24 h, or a ratio of 2.05% compared to total drugs encapsulated in the microneedle patches (Fig. 4f). This value is about 5 times higher than that achieved using microneedles without solution treatment, in agreement with the drug permeation described above (Fig. 4d) and suggesting the critical role of urea in permeation enhancement. Although 2% is lower than that reported for a variety of dissolving microneedles, this value is likely affected by the large proportion of drugs encapsulated in the backing region of SRT microneedles that do not directly permeate through the microchannels created by the microneedles. This value is also comparable to that of many commercially available formulations of transdermal drug delivery systems that often retain up to 95% of the initial amount of drug.[41]

Delivery of antibiotics

As a further proof-of-concept validation of the versatility of suckerin microneedles for drug carrier applications, we encapsulated kanamycin antibiotics within the microneedles and examined their antibiotic activity. First, in order to verify that the solvent used for microneedle processing (2% acetic acid) did not chemically degrade kanamycin – and therefore inhibit its biological activity – matrix-assisted laser desorption ionization time-of flight (MALDI-TOF) mass spectroscopy measurements were conducted. These measurements indicated that the molecular weight of kanamycin was not altered (Fig. S4a, ESI†), confirming no drug degradation. Kanamycin in 2% acetic acid was also investigated in *E. coli* cell studies, where we found no growth of bacteria compared to the control sample (Fig. S4b, ESI†). Loading of kanamycin within the suckerin microneedles resulted in visible inhibition of bacterial growth in the drug release diffusion region, which was effective in a larger area that spread out from the original location (Fig. 5a). In contrast, no obvious decrease in bacterial density was observed for the 3M microneedle control. Interestingly, a slight antibiotic effect was also observed for bare suckerin microneedles free of any antibiotics, as shown by cell growth inhibition (Fig. 5a). In order to verify this phenomenon and to quantitatively examine the antibiotic effects of the various types of microneedles, we conducted a slurry culture study and quantified the colony forming units (CFU) on each type of microneedles. After 24 h of culture, the density of *E. coli* on kanamycin-loaded suckerin microneedles was reduced to a negligible value of $\sim 5 \times 10^2$ CFU per mL (Fig. 5b and Fig. S5, ESI†), while that on 3M microneedles was $\sim 7.03 \times 10^7$ CFU per mL, demonstrating the excellent antibiotic ability of kanamycin-loaded suckerin microneedles. Cell density on kanamycin-free suckerin microneedles was also reduced to

 This journal is © The Royal Society of Chemistry 2017

Published on 12 September 2017. Downloaded on 15/11/2017 07:40:57.

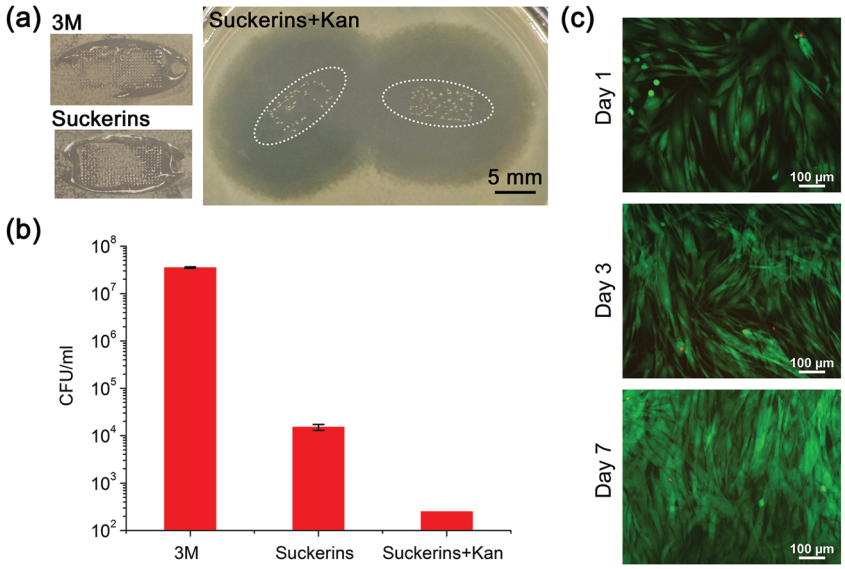

Fig. 5 (a) Representative photographs showing the inhibition of *E. coli* exposed to a commercial template, the suckerin microneedles, and the kanamycin-loaded suckerin microneedles (Kan: kanamycin). In the right panel, the dashed ellipses represent the original positions of Kan-loaded suckerin microneedles, while the dark surrounding region corresponds to extensive inhibition of bacterial growth by kanamycin released from the microneedles. (b) Average colony formation unit (CFU) counts for *E. coli* exposed to different microneedles in comparison with exposure to the template microneedles. (c) Live/dead assay of human dermal fibroblast (HDF) cells cultured on suckerin films.

$\sim 3.02 \times 10^4$ CFU per mL, thereby confirming the intrinsic antibiotic capacity of bare suckerin microneedles, though not as efficient as kanamycin-loaded suckerin microneedles. Notably, the antibiotic effect of suckerin microneedles (with more than 5 orders of magnitude decrease in cell density) was higher than that reported for other microneedles in antibiotics delivery application, such as silk fibroin microneedles[8] which only resulted in one order of magnitude drop in cell density. This result indicates that suckerin microneedles can serve as an efficient drug delivery system, and that they constitute a useful biomaterial to further prevent the risk of infection issues encountered in microneedle systems.[8,11]

As an additional control, we tested whether acetic acid itself could inhibit bacterial growth by conducting cell culture studies at various concentrations of acetic acid. A bacterial growth comparable to that of the control medium was found at 0.02% acetic acid or below. On the other hand, 0.2% acetic acid significantly decreased the bacterial cell density (Fig. S6a, ESI†). This observation was supported by the OD_{600} of cell culture, where 0.2% acetic acid resulted in a $\sim$75% reduction in OD_{600} compared to the lower acetic acid concentrations and the control (Fig. S6b, ESI†). While SRT were initially solubilized in 2% acetic acid before molding onto the PDMS template, microneedle curing is based on solvent evaporation of the highly volatile acetic acid, which was achieved by drying the sample for more than 5 days in the fumehood. Therefore, the final content of acetic acid is much lower than 0.2%, such that the antibiotic activity of bare suckerin microneedles is attributed to the suckerins themselves, and not to the bacterial growth inhibition of acetic acid. This antibiotic activity of suckerin proteins can be linked to their amino acid composition. Because of their relatively high content of His ($\sim$10 mol%, Fig. 1a), most suckerins exhibit an iso-electric point higher than 7, making them positively charged near neutral conditions of the cell culture medium, as previously demonstrated for recombinant suckerin-19.[42] Positively charged polymers, including biopolymers, are well-established to display antibiotic ability,[43] the classical example being that of chitosan.[44] Thus, we attribute the antibiotic effect of suckerin microneedles to the proteins' intrinsic physico-chemical characteristics. To verify this hypothesis, we conducted bacterial cell culture studies and added soluble suckerins in the medium (Fig. S7, ESI†). While suckerins were not able to inhibit the growth of *E. coli* at 0.3 mg mL^{-1} and below, a decrease in cell density was observed at 0.9 mg mL^{-1}. An equivalent concentration of acetic acid in the medium, on the other hand, failed to achieve this inhibition efficacy. These data support the antibiotic ability observed for bare suckerin microneedles, although we emphasize that loading of kanamycin within the microneedles led to a superior antibiotic activity.

Biocompatibility of suckerin microneedle arrays

Lastly, the biocompatibility of suckerin microneedles was established by *in vitro* cell culture studies (Fig. 5c). Flat films of suckerins were prepared using otherwise identical conditions as for microneedle samples. We selected human dermal fibroblast (HDF) cells for the study since they are located in the dermis layer of skins and would be in direct contact with suckerin microneedles in an actual skin patch. In agreement with previous studies on recombinant suckerin-19 based materials,[21] the live/dead assay indicated a homogeneous attachment of HDF cells, which started to spread extensively on the suckerin film from day 1 post-seeding. The cells continued to proliferate until they were almost confluent on day 7. Importantly, almost no dead HDF cells were detected. Overall, the easy cell attachment and

Published on 12 September 2017. Downloaded on 15/11/2017 07:40:57.

spreading, rapid proliferation, and long-term survival of HDF cells suggest that suckerin microneedles are non-cytotoxic and biocompatible, opening the door to their applications for drug delivery micro-devices without fundamental obstacles with regard to their safety.

For future therapeutic applications, the *in vivo* safety of suckerins used to fabricate our microneedles must also be substantiated. In a recent study,[38] we established that recombinant suckerin proteins were safe on *in vivo* mice models. Solutions of free suckerin proteins and drug-loaded suckerin nanoparticles did not induce acute reactions or toxicity in mice. No signs of skin irritation, including erythema and oedema, were observed after hypodermic injections of free suckerin protein and nanoparticles (besides the implanted subcutaneous tumor). In addition, no significant differences in body weight were detected between animals subjected to treatment with suckerins and control PBS solution after a period of 3 weeks, thus establishing the *in vivo* safety profile of suckerins.

Conclusions

In summary, we have used the recently discovered suckerin proteins to engineer microneedle arrays for sustained and tunable drug release for transdermal drug delivery applications. By exploiting the intrinsic block-copolymer like sequence design of suckerin proteins and their ability to self-assemble into a β-sheet supramolecular network, suckerin microneedles could be easily and efficiently fabricated by a soft lithography method. This allowed mild and drug/polymer friendly processing as well as the precise replication of geometrical parameters from the templates. Suckerin microneedles exhibit robust mechanical properties comparable to that of native SRT in dry conditions, which directly endow them with high skin penetration ability. Taking advantage of β-sheet disruption and the abundance of His residues of suckerins, a key finding is that the mechanical response of suckerin microneedles can be modulated over several orders of magnitude by simple variation of pH or by the addition of a hydrogen bond disruptor. These treatments lead to tailorability of secondary structure content within the suckerins, and consequently to the tuning of drug release profiles. *In vitro* skin permeation studies reveal a fast onset of drug permeation for suckerin microneedles, suggesting the critical role of microneedles in creating micro-channels in skin. The skin permeation over 24 h can be tuned *ca.* 10 times with the application of PBS and urea solutions and the permeation is higher than that with flat patches made of the same materials and prepared under identical conditions. With the application of PBS and urea solution, the total amount of drug permeated through and retained in the skin could be tuned and reached ~2% of total drug encapsulated into microneedles, which is comparable to the drug permeation percentage of commercial transdermal drug delivery systems. Lastly, native suckerin displays an intrinsic antibiotic ability, and this antibiotic efficacy can be strongly enhanced by loading the microneedles with kanamycin. Suckerin microneedles are also shown to be biocompatible in cell culture studies, opening the door for further clinical applications. We believe that suckerin-based microneedles would be able to successfully overcome current limitations associated with other metallic and polymeric microneedles, thus opening promising avenues in storage and transdermal delivery of therapeutics. The findings described in this work also further expand the space of applications of suckerin proteins in medicine, and provide molecular-scale design strategies that may be implemented for other types of modular structural proteins or supramolecular block co-polymers.

Experimental

Extraction and dissolution of suckerins

The extraction of suckerins from jumbo squid (*Dosidicus gigas*) SRT followed previously established protocols.[19] Briefly, suckerin powder was obtained by grinding SRT under liquid nitrogen and was then dried overnight in a chemical hood at room temperature. The ground suckerins were dissolved in 2% acetic acid (v/v) at 50 mg mL^{-1} by vigorous vortexing. The solution was then centrifuged at 19 000*g* for 5 min to remove trace amounts of insoluble particles. Suckerin solutions were stored at 4 °C until further use.

Fabrication of polydimethylsiloxane (PDMS) molds and suckerin microneedle arrays

A template microneedle array (3M™ Microchannel Skin System) (Fig. 2a) was used to fabricate an elastomer-based mold following an established soft-lithography method.[45] Briefly, polydimethylsiloxane (PDMS) solution was prepared by mixing the base and curing agents in a 10 : 1 (wt/wt) ratio. The solution was degassed and poured over the template structures to create a negative mold that exactly reverse-replicated the template structure and dimensions on curing at 70 °C for 2 h. Suckerin solution (800 μL for one patch) was then applied to the PDMS mold, covering the whole array area, and degassed in a vacuum chamber for 10 min at room temperature to fill the liquid into the microneedle mold. The solution was dried in a chemical hood with a constant wind speed of 0.3 m s^{-1} for 5 days or more to completely dry the solution and form the suckerin microneedle patch. The rhodamine B loaded suckerin microneedle patch was made in a similar way, where the protein solution was prepared by mixing 50 mg mL^{-1} suckerin with 10 mg mL^{-1} rhodamine (in water) at a 9 : 1 (v/v) ratio. The kanamycin loaded suckerin microneedle arrays were prepared in the same manner with a solution mixture containing 50 mg mL^{-1} suckerin and 30 mg mL^{-1} kanamycin (in water) at a 9 : 1 (v/v) ratio. The customized microneedle array template was achieved by a 3D printing method. Further experimental details are provided in ESI.†

Optical fluorescence imaging and scanning electron microscopy (SEM)

The optical images of suckerin microneedle arrays were taken with a digital camera (EOS 700D, Canon) equipped with a 100 mm micro lens, or with a stereomicroscope (Stemi DV4, Zeiss).

 This journal is © The Royal Society of Chemistry 2017

Published on 12 September 2017. Downloaded on 15/11/2017 07:40:57.

The morphology and dimension of 3M and suckerin microneedle arrays were also characterized by scanning electron microscopy (JSM-7600F, JEOL) at an accelerating voltage of 5 kV. Each sample was gold-coated with a sputter coater (JFC-1600, JEOL) for 30 seconds before imaging. The rhodamine B loaded microneedle arrays were imaged by stereo fluorescence microscopy (SMZ25, Nikon) with an excitation wavelength range of 530–560 nm.

Skin penetration efficiency of suckerin microneedle arrays

The *in vitro* skin penetration capability of suckerin microneedle arrays was investigated by using a loading applicator (JSV H1000, Algol Instrument). Rat skins were obtained *via* the animal tissue sharing program of the National University of Singapore. De-fatted rat skins were placed on top of 10 layers of kimwipes tissue paper to mimic a tissue-like mechanical support.[46] A force at 30 N was vertically applied to the microneedle arrays on top of the skin for 1 min and removed. The efficiency of skin penetration was examined by trypan blue staining.[13] Trypan blue solution (0.4 wt%) was loaded onto treated skins which were stained for 5 min, and the solution was gently removed with tissue paper. The skin was then imaged using a stereomicroscope (SMZ25, Nikon) to identify the microneedle penetration. The skin sample after microneedle penetration was also examined with SEM and H&E staining. Additional experimental details are provided in ESI.†

Mechanical properties of suckerin microneedle arrays

The mechanical properties of suckerin microneedle arrays were investigated by nanoindentation with a TriboScan 950 (Hysitron) nanoindenter following previously described procedures.[18,21] Suckerin microneedles were embedded in epoxy resin and cut by ultra-microtomy to obtain flat and smooth cross-section surfaces of single microneedles (Fig. S2a, ESI†). Microtomed samples were placed into a custom-made glass Petri dish designed for measurement under both dry and hydrated conditions. In dry conditions, cross-sections of SRT were probed with an elongated cube-corner tip (20 indents), with a maximum load of 50 μN, loading and unloading rates of 10 μN s^{-1}, and a holding time of 2 s at peak load. The Oliver–Pharr method was used to extract the elastic modulus (E) of microneedles.[47]

After the measurements in dry conditions, the samples were subjected to treatment with different solutions including a pH 5.0 buffer, 1× PBS at pH 7.4 and 2 M urea in water, respectively. Indentation in PBS was performed with a cube-corner tip, similar to testing in dry conditions.[18] In pH 5 buffer, since the samples were too soft to be probed by a sharp tip, the elastic modulus was obtained by Hertzian contact using an elongated cono-spherical tip (nominal radius of 9 μm) and a large extended displacement stage (×Z 500, Hysitron) capable of applying maximum displacement up to 500 μm. Suckerin microneedles were probed using the ''air indent'' method (30 s loading, 10 s unloading) under the ''Image'' mode. The indents were performed in the displacement control mode by imposing 3 to 7 μm displacement into the samples. The elastic modulus was calculated by fitting the initial loading portion of the indentation curves using the Hertz elastic solution for a blunt contact (Fig. S2b, ESI†).[29] The mechanical properties of suckerin microneedle arrays subjected to treatment with 2 M urea were characterized by rheological measurements using an Anton Paar MCR 501 rheometer (Anton Paar) equipped with a 10 mm parallel plate. The temperature was set to 20 °C and an amplitude sweep was first performed to determine the viscoelastic regime. Frequency sweeps from 0.1 to 10 Hz were then carried out to ensure that measurements occurred within the viscoelastic regime.

Fourier transform infrared spectroscopy (FTIR)

The secondary structure of suckerin microneedle arrays was measured by FTIR using a Bruker Vertex 70 infrared spectrometer (Bruker) in the Attenuated Total Reflection (ATR) mode. Each sample was scanned for 4 min with a resolution of 4 cm^{-1} and a wavenumber range of 400–4000 cm^{-1} at room temperature. Suckerin microneedle arrays were first measured in dry conditions, and then incubated in different solutions (pH 5.0 buffer, 1× PBS at pH 7.4 and 2 M urea) for at least 20 min before the measurements in each condition. The blank solutions were measured as controls and their spectra were used for subtraction with the OPUS software.

Drug release from suckerin microneedle arrays

Rhodamine loaded suckerin microneedle arrays were used for drug release studies under various conditions. The upper surface of the patch was covered with a waterproof vinyl tape (3M) to prevent diffusion of drugs from the upper surface[12] (which will be facing the air in the *in vivo* application). Afterwards, the suckerin microneedle patch was immersed in 4 mL of pH 5.0 acetate buffer (20 mM), pH 7.4 PBS and 2 M urea respectively in 15 mL falcon tubes, and incubated at 37 °C for drug release. At different time intervals (0.5 h, 1 h, 3 h, 6 h, 10 h, 24 h, 48 h, 72 h to 96 h) 2 mL solution was taken from each tube, which were replenished with 2 mL of fresh solutions. The rhodamine concentration in each sample was determined by using a plate reader (Infinite M200, TECAN) (excitation wavelength 553 nm; emission wavelength 627 nm) for the comparison of accumulative release of rhodamine in different solutions.

In vitro skin permeation study

To determine the drug delivery across skins by suckerin microneedles, an *in vitro* skin permeation study was conducted. With the approval from the National University of Singapore Institutional Review Board, human dermatome skin (65 year old male Caucasian) obtained from Science Care (Phoenix, AZ, USA) was used to determine the rate and extent of rhodamine B permeation through the skin from suckerin microneedles. Flat patches were used as controls and were prepared with similar protocols as suckerin microneedles, except that 3M templates were horizontally inverted during casting of PDMS molds to omit the microneedles and minimize the variations of sample size and shape (see section ''Fabrication of polydimethylsiloxane (PDMS) molds and suckerin microneedle arrays''). The human

Published on 12 September 2017. Downloaded on 15/11/2017 07:40:57.

skin sample was hydrated in 1× PBS for 30 min before use. In total 2 types of samples (microneedles and flat patches) with 4 different conditions (dry, PBS, 2 M and 4 M urea solutions, respectively) were tested. For the application of suckerin microneedles, 10 layers of Kimwipes tissue paper which mimic the underlying skin tissues were used to support the skin. The microneedle patches were cut and trimmed on the periphery to fit the size of Franz cells' donor chambers and applied on the skin for 30 s with a constant force of 30 N by a loading applicator (JSV H1000, Algol Instrument). The array was then secured onto the skin using medical grade porous tapes. Flat patches were fixed on the skins in a similar way without force loading. The skins with the patches were then mounted on Franz cells with an effective exposed area of 1 cm^2. The donor chambers were loaded with 2 mL of PBS or urea solutions, while the receptor chambers were filled with 4.8 mL of PBS. Afterwards, the Franz cells were maintained at 32 °C in an incubator, with the receptor solutions continuously stirred at 250 rpm with magnetic bars. The samples were collected at regular time intervals by taking out 2 mL of receptor solution at each time and replenishing with the same amount of fresh receptor solution. The samples were then stored at 4 °C and centrifuged at 12 000*g* for 3 min before the supernatant was withdrawn for analysis. The skin at the end of 24 h permeation was analyzed for the amount of rhodamine B retained in the skin. The skin was cut into fine pieces and homogenized with 1 mL of PBS, using pestle and mortar. Subsequently, 3 mL of methanol was added to it and the whole setup was sonicated for 20 min to extract Rhodamine B trapped in the skin. Finally, the samples were centrifuged as above before the supernatant was withdrawn for analysis. The amount of rhodamine B was quantified using a HPLC coupled with a fluorescence detector at an excitation/emission wavelength of 550/580 nm. An isocratic mode was used, with 71% methanol and 29% water at a flow rate of 1 mL per min using a Zorbax Eclipse XDB C18 column (Agilent, 5 μm, 4.6 × 150 mm). The average retention time for Rhodamine B was 6.1 min.

Delivery of antibiotics and anti-bacterial activity assessment

Suckerin microneedle arrays loaded with kanamycin were prepared as discussed above. LB medium (Merck) and LB-agar plates were prepared according to the manufacturer's instructions. *E. coli* cells were spread out from glycerol stocks following the instructions of the manufacturer. A 10 μL aliquot of stock cells was streaked onto LB agar plates and grown overnight at 37 °C. Single colonies were inoculated into LB media for overnight shaking at 37 °C to achieve an optical density (OD_{600}) at ~3.0. The cell culture was then diluted 3 times with fresh LB medium (corresponding to a viable count of approx. 10^8 CFU per mL) and 100 μL of diluted cell culture was inoculated onto one LB-agar plate. Afterwards, the 3M template, the suckerin microneedle arrays without antibiotics, and the suckerin microneedles loaded with kanamycin were applied on the LB-agar plates respectively (with the microneedles facing the plates), which were cultured at 37 °C for 24 h. The qualitative analysis of the antibiotic activity of various microneedle arrays was achieved by photographic imaging of each LB-agar plate after culture. The quantitative comparison of antibiotic efficiency between different microneedle arrays was investigated by a slurry culture method according to a previously established protocol.[48] Experimental details can be found in ESI.† The analysis of anti-bacterial effects of free suckerin proteins was performed in a similar way, with details also provided in ESI.†

Biocompatibility analysis

The *in vitro* cytotoxicity of suckerin microneedle arrays was evaluated by *in vitro* cell culture studies using a previously adopted method.[21] Human dermal fibroblast (HDF) cells were cultured in Dulbecco's Modified Eagle's Medium (DMEM) supplemented with 10% fetal bovine serum and 1% antibiotic/antimycotic (Life Technologies). Flat surface suckerin films were prepared for the biocompatibility analysis. Briefly, 80 μl of suckerin solution (50 mg mL^{-1} in 2% acetic acid) was loaded onto a cover slip and spread to an area around 1 cm × 1 cm. The samples were then dried in a chemical hood with a constant wind speed of 0.3 m s^{-1} for at least 3 days, which allowed the complete drying of the solution and the formation of solid films. The resultant suckerin films were incubated in 70% ethanol for 2 h for sterilization, washed with PBS multiple times to completely remove ethanol and then transferred to a low-binding 12-well plate (Nunc brand, Thermo Scientific). HDF cells were seeded at ~150 cells mm^{-2} and allowed to adhere for 12 h. All films were then transferred to fresh wells and refilled with 1 mL of fresh culture medium to ensure removal of cells attached on the bottom of the well and to continue the culture. At day 1, day 3 and day 7 post seeding respectively, the cytotoxicity of suckerin films was evaluated on HDF cells using a Live/Dead Viability/Cytotoxicity kit (Life Technologies) according to the manufacturer's directions. Cells were incubated with calcein AM and ethidium homodimer-1 (EthD-1) at 37 °C for 10 min to stain live (green) and dead (red) cells respectively. Cells were then imaged using a fluorescence microscope (Nikon Ti, Nikon) with excitation and emission wavelengths of 494 nm and 517 nm, respectively, for live cells. For dead cells, the excitation and emission wavelengths were 517 and 617 nm, respectively. Viable/living cells displayed strong green fluorescence whereas dead/non-viable cells displayed strong red fluorescence.

Conflicts of interest

The authors declare no competing financial interest.

Acknowledgements

We acknowledge financial support from a joint NRF-French Agence Nationale de la Recherche (ANR) collaborative grant awarded to A. M (NRF2015-NRF-ANR000-PREPROPOSAL) and from the Singapore Ministry of Education (MOE) through an Academic Research Fund (AcRF) Tier 1 grant (#MOE2015-T1-002-064). L. K. acknowledges funding from the Singapore MOE

 This journal is © The Royal Society of Chemistry 2017

Published on 12 September 2017. Downloaded on 15/11/2017 07:40:57.

AcRF Tier 1 grant (R-148-000-207-112). We thank Cesar Salinas, Cesar Salinas Jr, Admir Masic, and James Weaver for their help with SRT sample collection.

References

1 R. Langer, *Nature*, 1998, **392**, 5–10.
2 S. Khafagyel, M. Morishita, Y. Onuki and K. Takayama, *Adv. Drug Delivery Rev.*, 2007, **59**, 1521–1546.
3 S. P. Sullivan, N. Murthy and M. R. Prausnitz, *Adv. Mater.*, 2008, **20**, 933–938.
4 I. C. Lee, J.-S. He, M.-T. Tsai and K.-C. Lin, *J. Mater. Chem. B*, 2015, **3**, 276–285.
5 J. A. Mikszta, J. B. Alarcon, J. M. Brittingham, D. E. Sutter, R. J. Pettis and N. G. Harvey, *Nat. Med.*, 2002, **8**, 415–419.
6 W. Martanto, S. P. Davis, N. R. Holiday, J. Wang, H. S. Gill and M. R. Prausnitz, *Pharm. Res.*, 2004, **21**, 947–952.
7 Y. C. Kim, J. H. Park and M. R. Prausnitz, *Adv. Drug Delivery Rev.*, 2012, **64**, 1547–1568.
8 K. Tsioris, W. K. Raja, E. M. Pritchard, B. Panilaitis, D. L. Kaplan and F. G. Omenetto, *Adv. Funct. Mater.*, 2012, **22**, 330–335.
9 S. P. Sullivan, D. G. Koutsonanos, M. Del Pilar Martin, J. W. Lee, V. Zarnitsyn, S. O. Choi, N. Murthy, R. W. Compans, I. Skountzou and M. R. Prausnitz, *Nat. Med.*, 2010, **16**, 915–920.
10 S. P. Davis, B. J. Landis, Z. H. Adams, M. G. Allen and M. R. Prausnitz, *J. Biomech.*, 2004, **37**, 1155–1163.
11 E. Larrañeta, R. E. M. Lutton, A. D. Woolfson and R. F. Donnelly, *Mater. Sci. Eng., R*, 2016, **104**, 1–32.
12 J. S. Kochhar, W. X. Lim, S. Zou, W. Y. Foo, J. Pan and L. Kang, *Mol. Pharmaceutics*, 2013, **10**, 4272–4280.
13 J. Yu, Y. Zhang, Y. Ye, R. DiSanto, W. Sun, D. Ranson, F. S. Ligler, J. B. Buse and Z. Gu, *Proc. Natl. Acad. Sci. U. S. A.*, 2015, **112**, 8260–8265.
14 R. F. Donnelly, T. R. Singh, M. J. Garland, K. Migalska, R. Majithiya, C. M. McCrudden, P. L. Kole, T. M. Mahmood, H. O. McCarthy and A. D. Woolfson, *Adv. Funct. Mater.*, 2012, **22**, 4879–4890.
15 A. Miserez, J. C. Weaver, P. B. Pedersen, T. Schneeberk, R. T. Hanlon, D. Kisailus and H. Birkedal, *Adv. Mater.*, 2009, **21**, 401–406.
16 S. H. Hiew and A. Miserez, *ACS Biomater. Sci. Eng.*, 2017, **3**, 680–693.
17 P. A. Guerette, S. Hoon, Y. Seow, M. Raida, A. Masic, F. T. Wong, V. H. Ho, K. W. Kong, M. C. Demirel, A. Pena-Francesch, S. Amini, G. Z. Tay, D. Ding and A. Miserez, *Nat. Biotechnol.*, 2013, **31**, 908–915.
18 P. A. Guerette, S. Hoon, D. Ding, S. Amini, A. Masic, V. Ravi, B. Venkatesh, J. C. Weaver and A. Miserez, *ACS Nano*, 2014, **8**, 7170–7179.
19 V. Latza, P. A. Guerette, D. Ding, S. Amini, A. Kumar, I. Schmidt, S. Keating, N. Oxman, J. C. Weaver, P. Fratzl, A. Miserez and A. Masic, *Nat. Commun.*, 2015, **6**, 8313.
20 C. Rieu, L. Bertinetti, R. Schuetz, C. C. Salinas-Zavala, J. C. Weaver, P. Fratzl, A. Miserez and A. Masic, *Bioinspiration Biomimetics*, 2016, **11**, 055003.
21 D. Ding, P. A. Guerette, J. Fu, L. Zhang, S. A. Irvine and A. Miserez, *Adv. Mater.*, 2015, **27**, 3953–3961.
22 F. Tantakitti, J. Boekhoven, X. Wang, R. V. Kazantsev, T. Yu, J. Li, E. Zhuang, R. Zandi, J. H. Ortony, C. J. Newcomb, L. C. Palmer, G. S. Shekhawat, M. O. de la Cruz, G. C. Schatz and S. I. Stupp, *Nat. Mater.*, 2016, **15**, 469–476.
23 A. Ghadban, A. S. Ahmed, Y. Ping, R. Ramos, N. Arfin, B. Cantaert, R. V. Ramanujan and A. Miserez, *Chem. Commun.*, 2016, **52**, 697–700.
24 H. Li, Y. S. Low, H. P. Chong, M. T. Zin, C. Y. Lee, B. Li, M. Leolukman and L. Kang, *Pharm. Res.*, 2015, **32**, 2678–2689.
25 L. Fritz and D. Hofmann, *Polymer*, 1997, **38**, 1035–1045.
26 B. P. Koppolu, S. G. Smith, S. Ravindranathan, S. Jayanthi, T. K. Suresh Kumar and D. A. Zaharoff, *Biomaterials*, 2014, **35**, 4382–4389.
27 A. M. Römgens, D. L. Bader, J. A. Bouwstra, F. P. T. Baaijens and C. W. J. Oomens, *J. Mech. Behav. Biomed. Mater.*, 2014, **40**, 397–405.
28 R. L. Bronaugh, R. F. Stewart and E. R. Congdon, *Toxicol. Appl. Pharmacol.*, 1982, **62**, 481–488.
29 A. C. Fischer-Cripps, *Nanoindentation*, Springer, New York, 2011.
30 F. W. Zok and A. Miserez, *Acta Mater.*, 2007, **55**, 6365–6371.
31 H. J. Jin, J. Park, V. Karageorgiou, U. J. Kim, R. Valluzzi, P. Cebe and D. L. Kaplan, *Adv. Funct. Mater.*, 2005, **15**, 1241–1247.
32 S. Keten, Z. Xu, B. Ihle and M. J. Buehler, *Nat. Mater.*, 2010, **9**, 359–367.
33 Q. Lu, X. Hu, X. Wang, J. A. Kluge, S. Lu, P. Cebe and D. L. Kaplan, *Acta Biomater.*, 2010, **6**, 1380–1387.
34 J. Kong and S. Yu, *Acta Biochim. Biophys. Sin.*, 2007, **39**, 549–559.
35 S. Cai and B. R. Singh, *Biophys. Chem.*, 1999, **80**, 7–20.
36 S. H. Hiew, P. A. Guerette, O. J. Zvarec, M. Phillips, F. Zhou, H. Su, K. Pervushin, B. P. Orner and A. Miserez, *Acta Biomater.*, 2016, **46**, 41–54.
37 S. Y. Yang, E. D. O'Cearbhaill, G. C. Sisk, K. M. Park, W. K. Cho, M. Villiger, B. E. Bouma, B. Pomahac and J. M. Karp, *Nat. Commun.*, 2013, **4**, 1702.
38 Y. Ping, D. Ding, R. Ramos, H. Mohanram, K. Deepankumar, J. Gao, G. Tang and A. Miserez, *ACS Nano*, 2017, **11**, 4528–4541.
39 L. Bartosova and J. Bajgar, *Curr. Med. Chem.*, 2012, **19**, 4671–4677.
40 D. Voegeli, *Dermatol. Res. Pract.*, 2012, **18**, 13–15.
41 G. A. Van Buskirk, D. Arsulowicz, P. Basu, L. Block, B. Cai, G. W. Cleary, T. Ghosh, M. A. Gonzalez, D. Kanios, M. Marques, P. K. Noonan, T. Ocheltree, P. Schwarz, V. Shah, T. S. Spencer, L. Tavares, K. Ulman, R. Uppoor and T. Yeoh, *AAPS PharmSciTech*, 2012, **13**, 218–230.
42 D. Ding, P. A. Guerette, S. Hoon, K. W. Kong, T. Cornvik, M. Nilsson, A. Kumar, J. Lescar and A. Miserez, *Biomacromolecules*, 2014, **15**, 3278–3289.

43 F. Siedenbiedel and J. C. Tiller, *Polymers*, 2012, **4**, 46.
44 M. Kong, X. G. Chen, K. Xing and H. J. Park, *Int. J. Food Microbiol.*, 2010, **144**, 51–63.
45 D. B. Wolfe, D. Qin and G. M. Whitesides, *Methods Mol. Biol.*, 2010, **583**, 81–107.
46 J. H. Park, M. G. Allen and M. R. Prausnitz, *J. Controlled Release*, 2005, **104**, 51–66.
47 W. C. Oliver and G. M. Pharr, *J. Mater. Res.*, 1992, **7**, 1564–1583.
48 ASTM Committee E35 on Pesticides and Alternative Control Agents. Subcommittee E35.22 on Pesticide Formulations and Delivery Systems, *Standard Test Method for Determining the Activity of Incorporated Antimicrobial Agent(s) in Polymeric Or Hydrophobic Materials*, 2012.

Published on 12 September 2017. Downloaded on 15/11/2017 07:40:57.

This journal is © The Royal Society of Chemistry 2017